

Journal of Heat and Mass Transfer Research

Journal homepage: https://jhmtr.semnan.ac.ir

ISSN: 2383-3068



Research Article

Forced Convection Analysis of Mono-Hybrid Nanofluid Flow Through a 2D Channel with Double Consecutive Expansion in the Presence of Baffle

Mahmoud Jourabian a*, Mehrdad Raeesi b

^a Department of Mechanical Engineering, Tarsus University, Tarsus, 33400, Turkey ^b School of Automotive Engineering, Iran Univrsity of Science and Technology, Tehran, 16846-13114, Iran

ARTICLE INFO

Article history:

Received: 2024-12-02
Revised: 2025-04-11
Accepted: 2025-04-27

Keywords:

DBFS;

HyNf;

Turbulent forced convection;

Baffle;

PEC;

OpenFOAM.

ABSTRACT

The fluid flow over two backward-facing steps (BFS) in series, called the double backwardfacing step (DBFS), is a quintessential geometry in industrial applications. An improved mixing and heat transfer performance is often essential, and this is accomplished by applying passive flow-control methods. In this paper, the thermal-hydraulic performances of using ND/water nanofluid (NF), ZrO2/water NF, water-based rGO/ND hybrid NF (HyNf) with the temperature-dependent properties in a horizontal DBFS channel equipped with an adiabatic baffle placed vertically downward from the top wall are evaluated. The k- ω SST model in OpenFOAM is employed to solve the governing equations for the single-phase turbulent forced convection heat transfer problem. For the pure water in the DBFSO channel (without a baffle), as the velocity of the incoming flow raises from 0.11 to 0.2, the friction factor abates by 20%. At Re=9900, when the adiabatic baffle is installed over the first downstream wall (DBFS1), the values of Nu_{max} over the first and second downstream walls enhance by 72% and 30%, respectively, compared to the BFS0 channel. Inserting an adiabatic baffle over the second heated downstream wall significantly enhances the average Nu number (by 28-31%) in contrast to the canonical case. In the DBFS1 and DBFS2 channels, the friction factor is higher than that in the canonical case by 43.24% and 304%, respectively. When the pure water is substituted with the above NFs (with ϕ =0.004 or 0.01), the value of the performance evaluation criterion (PEC) is lower than 1.0 in the turbulent separated flow. The use of an adiabatic baffle in an effective position (DBFS1) enhances the thermal efficacy of the system where a disadvantageous working fluid (with FOM1<1.0) is used. The simultaneous substitution of the base fluid in the DBFS0 channel with the single/hybrid NF in the DBFS1 or DFS2 channel is ineffective.

© 2025 The Author(s). Journal of Heat and Mass Transfer Research published by Semnan University Press. This is an open access article under the CC-BY-NC 4.0 license. (https://creativecommons.org/licenses/by-nc/4.0/)

1. Introduction

The separated flows, which are apparent in several technological applications such as cooling of electronic modules, microchannel heat sinks, automotive systems, heat exchangers, and diffusers, proved to be advantageous in terms of heat transfer improvement. Heat exchange and fluid mixing are boosted due to the appearance of

turbulent structures in such flows. For the BFS flow, there is a separation region created by the abrupt contraction (expansion). It creates a recirculation region (recirculating vortices) behind the step. Nevertheless, regions of separated flows are not always in isolation, and complex interactions between various regions occur. A DBFS channel is an arrangement of double steps with the distance between them in

E-mail address: mjourabian@tarsus.edu.tr

Cite this article as:

Jourabian, M. and Raeesi, M., 2025. Forced Convection Analysis of Mono-Hybrid Nanofluid Flow Through a 2D Channel with Double Consecutive Expansion in the Presence of Baffle. *Journal of Heat and Mass Transfer Research*, 12(2), pp. 301-321.

^{*} Corresponding author.

the streamwise direction as a changeable variable. Regarding the double-step arrangement, various recirculation zones are formed that modify the thermal-hydraulic features of the energy systems.

Tinney and Ukeiley [1] examined the flow characteristics over a 3D DBFS utilizing a particle image velocimetry (PIV) device and qualitative oil-flow visualizations. Compared to the typical 2D BFS flows, the fluctuating turbulent energy was found to be higher. The horseshoe vortex was produced instantly downstream of the first step by joining two spiral separation points. The unsteady shedding events were transmitted downstream along the shear layer toward the reattachment point. Due to the existence of counter-rotating vortices formed by negative stream-surface bifurcation, they were discarded from the surface.

Using a wall-resolved LES, Rao et al. [2] scrutinized the air-wake of a generic ship model (as a DBFS) at Re=8×104. It was found that the mean flow topology on the first step was antisymmetrical to the flow topology on the second one, and the two flow states were antisymmetrical to each other. The asymmetrical flow was generated by dissimilarity in the strength of longitudinal vortices along the edges of the first one.

Utilizing FVM-based the k-ε model, Abdulrazzaq et al. [3] explored the heat transfer enhancement in a double backward-facing expanding channel filled with water, ammonia liquid, and ethylene glycol at 98.5<Re<512. The top and bottom walls of the upstream region were assumed thermally insulated, whereas the walls of both steps were heated with a uniform heat flux q=2000.0 W/m². Compared to water and ammonia, the highest Nuave (representing the thermal performance) was achieved when EG was used and the dimensions of both steps were identical. An intensification in the local skin friction coefficient at both steps was reported because of the channel expansion (generated separation).

McQueen et al. [4] experimentally confirmed that the fluid flow over a DBFS with equal-height steps can be split into three flow regimes called single, intermediate, and double reattachment. For separations of less than four step heights, a single reattachment regime was detected, and there was an insignificant variation in fundamental flow characteristics compared to a single BFS response. For a separation of four step heights, an intermediate regime was recognized. Finally, for larger separations, a double reattachment regime with reattachment on both steps was detected. There was a downstream impact of the first recirculation region on the second one. As a result, the length of the second

region was reduced. The dynamic characteristics of the second region were affected by the large-scale structures created in the upstream recirculation region that persisted downstream of the second step. Furthermore, there was an upstream effect of the second zone on the first one. It resulted in a decrease of the first-step base pressure.

Mohankumar and Prakash [5] applied a finite element method (FEM)-based code to analyze the fluid flow and heat transfer in a DBFS channel with/without elliptical obstacles adjacent to steps. The motivation was to modify the corner recirculation (diminishing the impact of hotspots engendered by recirculation zones in convective flows with separation) to attain higher heat transfer performance. From a heat transfer point of view, the highest amplification in the local Nu number close to the steps was reported when the vertical location of the obstacles was equal to 0.769 with the axis ratio of 1.0 at Re=1000.0. The lowest size of the recirculation zone was recorded for the vertical location of 0.385.

Efforts to control separated flows have been commonly demanded for decades. The main goal is to increase the heat transfer and fluid-dynamic-related performances. Passive flow-control methods include the application of a magnetic field [6], ribbed/grooved channels [7], surface roughness [8], baffles/obstacles [9-12], rotating plate [13], and dispersion of NPs [14-15].

and Saha [16] numerically researched the hydro-thermal properties of water/FMWCNT NF flow in a BFS channel equipped with a baffle under a constant heat flux. Moreover, at a weight percentage of 0.25 and Re = 150, the percentage increase in the average Nu number and friction factor was equal to 47.37 and 11, respectively, for the BFS channel with a plane obstacle compared to the smooth channel (without a baffle). The increment of the Re number caused an augmentation in the boundary layer (BL) thickness; as a result, the value of the friction factor was reduced.

Nie et al. [17] numerically investigated the 3D laminar forced convection flow in a rectangular BFS channel with a baffle at Re=343. The value of Nu_{max} for D=1.0 (normalized streamwise distance of the baffle from the step or inlet region) was about three times of the one for the BFS channel without a baffle. Furthermore, the friction coefficient on the stepped wall was reduced as the baffle distance (D) was increased.

Heshmati et al. [18] numerically simulated 2D laminar mixed convection flow over a BFS equipped with different slotted baffles on the top wall for the water-based SiO₂, Al₂O₃, CuO and ZnO NFs ($1.0\% \le \phi \le 4\%$ and $20 \text{nm} \le d_p \le 50.0$ nm). It was reported that the inclined baffle gave the highest Nu number for $50 \le \text{Re} \le 400$, although it

imposed the highest pressure drop which was a drawback for this configuration. On the other hand, the inclined slotted baffle gave a lesser Nu number while it gave the minimal pressure drop as the Re number was increased. All types of NF possessed a higher Nu number than the base fluid (water). More specifically, the water/SiO₂ NF provided the highest local Nu number. Compared to the base fluid, the value of Nu_{max} was enhanced by 69% by using the water/SiO2 NF with ϕ =4% and d_p =20nm. Regarding the pressure drop and skin friction coefficient, there was a minimal difference between SiO2 and other NFs. Heshmati et al. [18] concluded that NFs with high density and low specific heat gave a higher Nu number, while NFs with low density and high specific heat gave a lower Nu number.

Alkumait et al. [19] numerically examined the influence of baffle position on the laminar forced convection flow over a 3D BFS in terms of Nu number and skin friction. It was discovered that the maximum Nu number was shifted in the downstream direction as the distance between the baffle and the inlet section increased. The highest Nu number and skin friction were achieved when the distance between the step and baffle was equal to 40 mm. The lowest ones were obtained by using the BFS channel without a baffle. Moreover, the highest rise of the average Nu number was about 213% at d=40 mm compared to the BFS channel without a baffle.

Li et al. [20] numerically studied the heat transfer characteristics for the laminar forced convective flow over a BFS in a rectangular horizontal channel equipped with a porous baffle. By increasing the Re number from 100 to 500, the value of Nu_{max} was enhanced by 2.5 times. Li et al. [20] found that in the best condition, the average Nu number was improved by 35%, while the pressure drop boosted about eight times. It must be stressed that this increment of the pressure drop was never reported by other researchers.

Eslami and Karbalaei [21] analyzed the steady incompressible laminar fluid flow (Pr=0.71) over a 2D BFS channel with ER = 2.0 (the bottom wall was partially heated at a constant heat flux) at Re=100.0. To satisfy the maximum temperature constraint (MTC), it was necessary that the fluid flow was not separated from the heated wall or the re-separation was sufficiently postponed. Eslami and Karbalaei [21] evaluated the merits of the baffle installation technique by computing a parameter called the performance evaluation parameter (PEP). Since the baffle installation did not satisfy the MTC (as a shortcoming), a small gap between the installation point of the inclined baffle and the top wall was imposed. Considering the simultaneous effects of a single solid baffle on the heat transfer and the required pumping

power, the case (X, Y, angle) = $(0.3, 0.9, 30^{\circ})$ was the recommended one (PEP = 1.257).

The laminar forced convection flow of Cu/water NF over a BFS with a baffle installed on the top wall was explored numerically by Moayedi et al. [22]. By enhancing the Re number and diminishing the concentration of copper NPs, the value of PEC was improved. It was reported that the Nuave and PEC were higher when the width of the baffle was equal to twice the height of the entrance region (H) compared to other widths (H, $3.0\times H$, $4.0\times H$). At Re<400.0, using two baffles was preferred over one, three, or four baffles considering the PEC and the ratio of Nuave between NF and base fluid.

Rana et al. [23] examined the thermalhydraulic characteristics of CuO/water NF $(0.0 \le \varphi \le 0.05 \text{ and } d_p = 20.0 \text{ nm})$ in a micro-scale channel with/without a baffle 100.0≤Re≤389.0. The increment of the volume fraction and Re number boosted the Nu number. Nevertheless, the skin friction coefficient was reduced with the augmentation of the Re number. Rana et al. [23] proposed that there is an optimum position and height of the baffle in specific flow conditions while the heat transfer is considerably enhanced. When the baffle was elongated, the Nu number was steadily improved. Also, the elongated baffle decreased the primary recirculation zone formed behind the step, while it enlarged the size of the secondary recirculation region behind the baffle. As the distance between the baffle and the step increased, the Nu number was reduced, while the size of the primary recirculation region was enlarged. Rana et al. [23] concluded that the improved heat transfer was accompanied by the penalty of augmented pumping power requirements.

It should be emphasized that the thermal performance (represented by FOM and PEC) of the working NFs is verified when the thermophysical properties of NFs are carefully evaluated at different temperatures and NP loadings. The primary variables required to explore the convection heat transfer characteristics are the viscosity, thermal conductivity, density, and specific heat. Sharma et al. [24] used the experimental data of the NF dynamic viscosity for φ≤3.7% 20nm≤d_p≤150nm from various works in the literature, and they were subjected to regression. Finally, a temperature-dependent correlation for the dimensionless effective dynamic viscosity of water-based NF was recommended. Sharma et al. [24] also developed regression correlation for the determination of thermal conductivity of waterbased NFs based on available experimental data (252 data points) for spherical NPs with a size of 20-150 nm, temperature of 20≤T≤70°C, and φ≤0.04. The influence of NP material on the NF

thermal conductivity data was considered through the thermal diffusivity ratio of NPs to the base fluid (water).

Palm et al. [25] stated that the resulting correlations obtained from the polynomial curvefitting on experimental records of properties were applicable for specific types of NFs within certain temperature ranges.

2. Research Gap and Objective

It is worth noticing that no one has investigated the accuracy of existing semiempirical models to estimate the NF properties compared to relevant experimental data in terms of the temperature-dependent FOM. To precisely verify the heat transfer benefits of NFs, Sundar et al. [26] suggested that an experimental study is needed. Accordingly, the temperature-dependent thermophysical properties of NFs can be precisely estimated, and a more dependable outcome is established. On the other hand, Prabakar et al. [27] proposed that the passive flow control techniques (baffles) can be employed to modify the recirculation regions in the separated flows. Then, less effective working fluids (for example, NFs with a FOM lower than 1.0) could become a preferable alternative.

Table 1 provides a valuable summary of the previous works that reported the values of FOM (Mo number-based) for the single/hybrid NFs. To the best knowledge of authors, there is no research in the literature investigating the effects of adiabatic baffle and single/hybrid NF with temperature-dependent properties on the single-phase turbulent forced convection heat transfer in a horizontal DBFS channel in terms of FOM and PEC.

In this paper, the benefits of using single/hybrid NFs (ϕ =0.004, 0.01) and an adiabatic baffle placed vertically downward from the top wall of a horizontal DBFS channel (with ER=3) are evaluated based on the value of PEC. The channel contains two equal-sized steps spaced up to thirty step sizes apart. A constant heat flux $(q=3000 \text{ W/m}^2)$ is imposed at the first and second downstream walls of the channel while the velocity of the incoming flow is in the range of $0.11 \le U_{ref} \le 0.2$. The thermophysical properties of ND/water NF, ZrO₂/water NF and water-based rGO/ND HyNF are temperaturedependent, and they are obtained from the available lab-scale measurements in the literature. Additionally, to check the validity of theoretical predictions of the NF properties, the value of FOM (based on the Mo number and a constant flow velocity comparison) is assessed. The validities of correlations given by Sharma et al. [24] are checked. The RANS and energy equations for the single-phase turbulent forced convection heat transfer in the separated flow are solved using the k-ω SST model in the opensource code OpenFOAM [36-38]. Moradi et al. [39] compared the results derived from singlephase (homogeneous) and two-phase (VOF) approaches with the experimental data for the laminar flow of Cu/water NF through BFS channels affected by a transverse magnetic field. Moradi et al. [39] found that except for strong magnetic fields, the single-phase approach remained suitable for predicting hydrothermal behavior of NF flow in a BFS channel. Moreover, Sekrani et al. [40] concluded that the single-phase SST k-ω model can be used to well account for the heat transfer close to the walls while appropriate correlations for the thermophysical properties of NFs at low volume fractions ($\phi \le 0.008$) should be implemented.

Table 1. Summary of works that reported the values of PEC_{nf} and FOM1 for NFs.

Ref.	Type of NF	Range of variables	FOM1	PEC_{nf}
Sundar et al. [26]	W/EG-based rGO/ND HyNf	0.2%≤ φ ≤1.0% and 20°C≤T≤60°C	FOM<1.0	-
Prabakar et al. [27]	Al ₂ O ₃ /W, TiO ₂ /W NF	0.05%≤ φ ≤0.2% and 20°C≤T≤60°C	FOM>1.0 at T>30°C	1.0≤PEC≤1.18
Leena and Srinivasan [28]	W/EG mixture-based TiO ₂ NF	0.1%≤ φ ≤0.8% and 10°C≤T≤70°C	FOM>1.0	-
Bianco et al. [29]	Al ₂ O ₃ /W NF	0.0%≤ φ ≤6.0%	-	PEC<1.0
Xuan et al. [30]	Al ₂ O ₃ -Cu-CuO/W ternary NFs	ф=0.02%	-	1.1≤PEC≤1.7
Rejvani et al. [31]	SiO ₂ /WNF	0.0%≤ φ ≤1.5% and 25°C≤T≤50°C	FOM<1.0	-

Ahmad et al. [32]	CuO/W, Al ₂ O ₃ /W and TiO ₂ /W NF, Al ₂ O ₃ -CuO/W and Al ₂ O ₃ - TiO ₂ /W HyNf	1.0%≤ φ ≤3.0%	1.2≤F0M≤1.25	1.1≤PEC≤1.67
Colla et al. [33]	Fe ₂ O ₃ /W NF	0.05%≤ φ ≤0.2% and 10°C≤T≤70°C	F0M<1.0	-
Ho et al. [34]	Al ₂ O ₃ /W NF	0.0%≤ φ ≤0.9% and 25°C≤T≤50°C	-	PEC<0.99
Kumar et al. [35]	MWCNT/W-based Al ₂ O ₃ , TiO ₂ , ZnO and CeO ₂ HyNf	0.25%≤ φ ≤2.0% and 25°C≤T≤50°C	Maximum FOM=1.16 for CeO ₂ HyNf	-

3. Numerical Model

3.1. Flow Geometry and Boundary Conditions

The horizontal DBFS channels investigated here are depicted in Figure 1. In the first channel called DBFS0, there is no adiabatic baffle. In the DBFS1 configuration, there is an adiabatic baffle (with a length of 0.041m) over the first downstream wall. In the DBFS2 channel, there is an adiabatic baffle (with a length of 0.082m) over the second downstream wall. In other words, compared to the DBFS1 channel, the adiabatic baffle is elongated and moves in the streamwise direction (moves further downstream) in the DBFS2 channel. The height of steps is equal to s=0.041m, and the height of the inlet region is equal to s=0.041m.

According to Jokari et al. [29], the reattachment length in flows over a BFS is changed by both the Re number and ER. In this study, the ER of the DBFS channel is fixed (3.0) and the streamwise step separation is constant (30×s). The temperature of the incoming fluid is T=293.0K. A constant heat flux of $q=3000~W/m^2$ is imposed at two downstream walls and the second vertical step. All walls of the channel are

assumed smooth. The remaining walls, including the baffle, are assumed adiabatic. The operating fluids are the pure water and ND/water NF, ZrO_2 /water NF and water-based rGO/ND HyNF with $0 \le \phi \le 0.01$.

For the pure water flow in DBFS channels, three different Reynolds numbers (5800, 7100, and 9900) are considered. The Re number is defined based on the step height and streamwise velocity at the center line of the upstream section. Based on the literature, the bulk flow is fundamentally 2D at Reynolds numbers Re < 400 and Re > 6000. Between these Re numbers, the flow is strongly 3D but continuously symmetric about the center plane of the test section.

The streamwise velocity at the center line is obtained at X=4.346m. The length of the inlet region is equal to L_1 =110×s. Note that the incoming flow (the inflow condition) is a fully developed turbulent flow [41], and hence, no numerical computation suffers from the incompleteness or ambiguity in the upstream region.

According to the literature review presented above, the width of the baffle mainly affects the flow field and heat transfer over the top wall, and hence, it is fixed in this study.

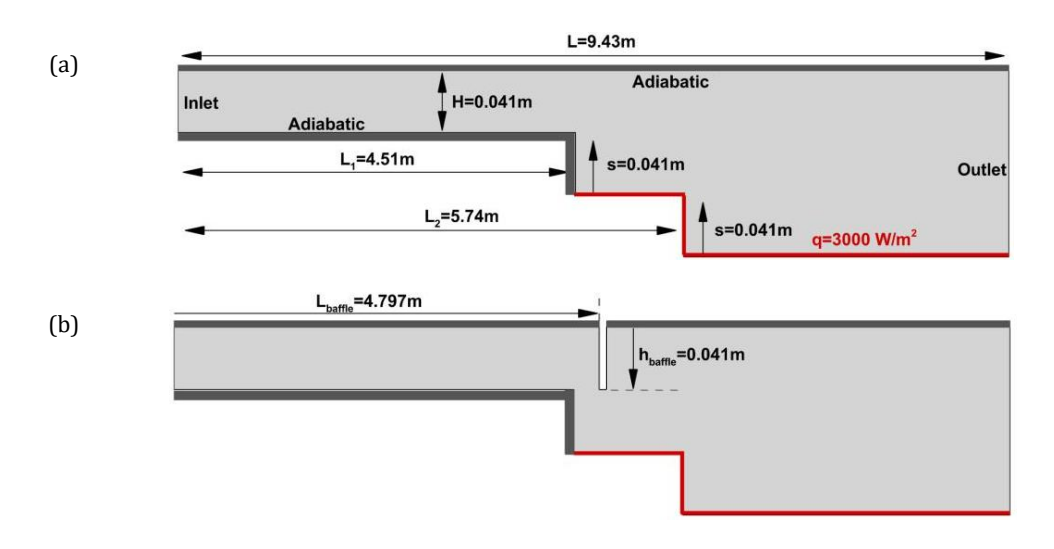


Fig. 1. Physical model of the present study considering various positions of the adiabatic baffle, (a) DBFS0, (b) DBFS1 and (c) DBFS2

3.2. Flow Geometry and Boundary Conditions

The horizontal DBFS channels investigated here are depicted in Figure 1. In the first channel called DBFS0, there is no adiabatic baffle. In the DBFS1 configuration, there is an adiabatic baffle (with a length of 0.041m) over the first downstream wall. In the DBFS2 channel, there is an adiabatic baffle (with a length of 0.082m) over the second downstream wall. In other words, compared to the DBFS1 channel, the adiabatic baffle is elongated and moves in the streamwise direction (moves further downstream) in the DBFS2 channel. The height of steps is equal to s=0.041m, and the height of the inlet region is equal to s=0.041m.

$$\frac{\partial \overline{u}_i}{\partial x_i} = 0.0 \tag{1}$$

$$\frac{\partial \overline{u}_{i}}{\partial t} + \frac{\partial \overline{u_{i}u_{j}}}{\partial x_{j}} = -\frac{1}{\rho_{nf}} \frac{\partial \overline{p}}{\partial x_{i}} + \nu_{nf} \frac{\partial^{2} \overline{u}_{i}}{\partial x_{i}^{2}} + \frac{1}{\rho_{nf}} \frac{\partial (-\rho_{nf} \underline{u}_{i} \underline{u}_{j})}{\partial x_{i}} \tag{2}$$

$$\frac{\partial \overline{T}}{\partial t} + \frac{\partial \overline{u_j T}}{\partial x_j} = \frac{\nu_{nf}}{P r_{nf}} \frac{\partial^2 \overline{T}}{\partial x_i^2} + \frac{1}{\rho_{nf}} \frac{\partial \left(-\rho_{nf} \overline{T} \hat{u}_j\right)}{\partial x_j} \tag{3}$$

In this study, the single-phase model (mixture continuum formulation) is adopted for the turbulent forced convection heat transfer in single/hybrid NFs.

The following assumptions are considered:

- The shape of dispersed NPs is spherical with a homogeneous size, and they are neutrally buoyant in NFs.
- (2) The water-based NFs are homogenous, behaving as a Newtonian fluid.
- (3) The flow inside the DBFS ducts is supposed to be incompressible with insignificant viscous dissipation.
- (4) Local thermodynamic equilibrium is considered between NPs and water.
- (5) All thermophysical properties of NFs are temperature-dependent.
- (6) The conduction effect within the walls of the channel is disregarded.

3.3. SST k- ω Model

Park [33] found that although the RANS model could not produce the turbulent fluctuations in BFS flows, the time-averaged velocity profile showed a reasonable agreement with the experimental data.

The difference between the SST $k-\omega$ model [43-44] and the original $k-\omega$ model is that an extra cross-diffusion term appears in the specific dissipation rate equation and, the constants are dissimilar. The Wilcox $k-\omega$ model is then multiplied by a function F_1 and transformed one by a function F_1 , and then we sum them. The function F_1 is equal to one close to the wall (activating the Wilcox $k-\omega$ model) and zero away from the surface.

The blending operation is considered in the wake region of the BL, and the model constants are evaluated using interpolation of appropriate inner and outer variables [45-47],

$$\Gamma = F_1 \Gamma_1 + (1.0 - F_1) \Gamma_2 \tag{4}$$

Note that Γ_1 is any constant in the Wilcox k- ω model and Γ_2 is any constant in the transformed k- ϵ model, and hence, Γ is the corresponding constant in the SST k- ω model. The eddy viscosity is defined by [45-47],

$$v_t = \frac{\mu_t}{\rho_{nf}} = \frac{k}{\omega} \tag{5}$$

In the concept of eddy viscosity (Boussinesq hypothesis), the turbulence stress tensor is given by [45-47],

$$\tau_{ij} = \rho_{nf} \overline{\dot{u}_i \dot{u}_j} ,$$

$$\tau_{ij} = -\frac{2}{3} \delta_{ij} + \mu_t \left(\frac{\partial \overline{u_i}}{\partial x_i} + \frac{\partial \overline{u_j}}{\partial x_i} \right)$$
(6)

For the wake region of the BL (with the adverse pressure gradient), the eddy viscosity is modified to account for the transport of the turbulent shear stress,

$$v_t = \frac{a_1 k}{max(a_1 \omega, SF_2)}, a_1 = 0.31,$$

$$S = \sqrt{S_{ij} S_{ij}}$$
(7)

Note that S is the characteristic magnitude of the mean velocity gradients. The governing equations for the turbulence kinetic energy (TKE) and specific dissipation rate (ω) in the SST k- ω model are written as [45-47],

$$\frac{\partial(\rho_{nf}k)}{\partial t} + \frac{\partial(\rho_{nf}\overline{u}_{j}k)}{\partial x_{j}} = min\left(2.0 \times \mu_{t}S_{ij}.S_{ij} - \frac{2}{3}\rho_{nf}k\frac{\partial u_{i}}{\partial x_{j}}\delta_{ij}, 10.0 \times \beta^{*}\rho_{nf}k\omega\right) + \frac{\partial}{\partial x_{j}}\left[\left(\mu_{nf} + \sigma_{k}\mu_{t}\right)\frac{\partial k}{\partial x_{j}}\right] - \beta^{*}\rho_{nf}k\omega$$
(8)

$$\frac{\partial(\rho_{nf}\omega)}{\partial t} + \frac{\partial(\rho_{nf}\overline{u}_{j}\omega)}{\partial x_{j}} = \frac{\partial}{\partial x_{j}} \left[\left(\mu_{nf} + \sigma_{\omega}\mu_{t} \right) \frac{\partial\omega}{\partial x_{j}} \right] + \gamma \left(2.0 \times \mu_{t}S_{ij}.S_{ij} - \frac{2}{3}\rho_{nf}\omega \frac{\partial u_{i}}{\partial x_{j}}\delta_{ij} \right) \\
-\beta\rho_{nf}\omega^{2} + 2.0 \times (1.0 - F_{1})\sigma_{\omega 2} \frac{\rho_{nf}}{\omega} \frac{\partial k}{\partial x_{j}} \frac{\partial\omega}{\partial x_{j}} \tag{9}$$

Note that S_{ij} , F_1 and F_2 are the strain rate tensor, and blending functions, respectively. In Table 2, all the coefficients of the numerical model are given.

Table 2. List of constants in the SST $k-\omega$ turbulence model [43-44].

$oldsymbol{eta}^*$	σ_{k1}	$\sigma_{\omega 1}$	$oldsymbol{eta}_1$	$oldsymbol{eta}_2$	κ	$\sigma_{ m k2}$	$\sigma_{\omega 2}$	γ_1	γ_2
0.09	0.5	0.5	0.075	0.0828	0.41	1.0	0.856	0.55	0.44

The other constants are defined as follows,

$$\gamma_1 = \frac{\beta_1}{\beta^*} - \frac{\sigma_{\omega 1} \kappa^2}{\sqrt{\beta^*}}, \qquad \gamma_2 = \frac{\beta_2}{\beta^*} - \frac{\sigma_{\omega 2} \kappa^2}{\sqrt{\beta^*}}$$
 (10)

The blending functions F_1 and F_2 are calculated based on [45-47],

$$F_1 = \tan h(\Phi_1^4), \quad F_2 = \tan h(\Phi_2^2)$$
 (11)

$$\Phi_{1} = min \left[max \left(\frac{\sqrt{k}}{\beta^{*} \omega y}, \frac{500 v_{nf}}{y^{2} \omega} \right), \frac{4 \rho_{nf} \sigma_{\omega 2} k}{C D_{k\omega} y^{2}} \right]$$
(12)

$$CD_{k\omega} = max \left(2\rho_{nf} \sigma_{\omega 2} \frac{1}{\omega} \frac{\partial k}{\partial x_i} \frac{\partial \omega}{\partial x_j}, 10^{-20} \right)$$
 (13)

$$\Phi_2 = max \left(\frac{2\sqrt{k}}{0.09\omega v}, \frac{500\nu_{nf}}{v^2\omega} \right) \tag{14}$$

Keep in mind that y is defined as the distance to the closest wall and F_1 is equal to zero away from the surface, and it is equal to unity inside the BL

4. Thermophysical Properties of NFs

In this study, the objective is to realize the effects of ND/water NF, ZrO2/water NF and water-based rGO/ND HyNF on the turbulent forced convection heat transfer over a DBFS channel with/without an adiabatic baffle.

To achieve it, the thermophysical properties of the above NFs must be carefully predicted and then included in numerical simulations. The thermophysical properties of all NPs in this study are provided in Table 3.

4.1. Semi-Empirical Model

The regression correlations were proposed by Sharma et al. [24] for predicting the dynamic viscosity and thermal conductivity of waterbased NFs,

Table 3. Thermophysical properties of single/hybrid NPs at T=20.0°C [26, 48-49]

Properties	ND	ZrO ₂	rGO	rGO/ND (70:30%)
k (W/m K)	1000.0~2200.0	1.70	4000.0	3460.0
ρ (kg/m ³)	3100.0	5680.0	1910.0	2267.0
c_p (J/kg K)	516.0~610.0	420.0	710.0	680.0

$$\mu_{nf} = \mu_{bf} \left[(1.0 + \phi)^{11.3} \left(1.0 + \frac{T_{nf}}{70.0} \right)^{-0.038} \left(1.0 + \frac{d_{np}}{170.0} \right)^{-0.061} \right]$$
 (15)

$$k_{nf} = k_{bf} \times 0.8938 \times \left[(1.0 + \phi)^{1.37} \left(1.0 + \frac{T_{nf}}{70.0} \right)^{0.2777} \left(1.0 + \frac{d_{np}}{150.0} \right)^{-0.0336} \left(\frac{\alpha_{np}}{\alpha_{bf}} \right)^{0.01737} \right]$$
(16)

4.1. Experimental Data

With the inherent restrictions associated with the theoretical predictions, the thermophysical properties of the above NFs were evaluated experimentally in the literature. The effects of the temperature and volume fraction of NPs on the thermophysical properties of various NFs are shown in Figure 2. The thermophysical properties of the base fluid (water) are temperature-dependent and given by ASHRAE [50].

Sundar et al. [26] experimentally evaluated the thermophysical properties of rGO-ND/water HyNf as well as their FOM at different particle volume loadings and temperatures.

Alklaibi et al. [48] experimentally predicted the thermophysical properties (thermal conductivity, viscosity, specific heat, and density) of the ND/water NF.

Sundar et al. [49] experimentally analyzed the thermophysical characteristics (thermal conductivity, viscosity, dynamic density, and specific heat) of ZrO_2 /water NFs in the range of $0.002 \le \varphi \le 0.01$ and $20^{\circ}C \le T \le 60^{\circ}C$.

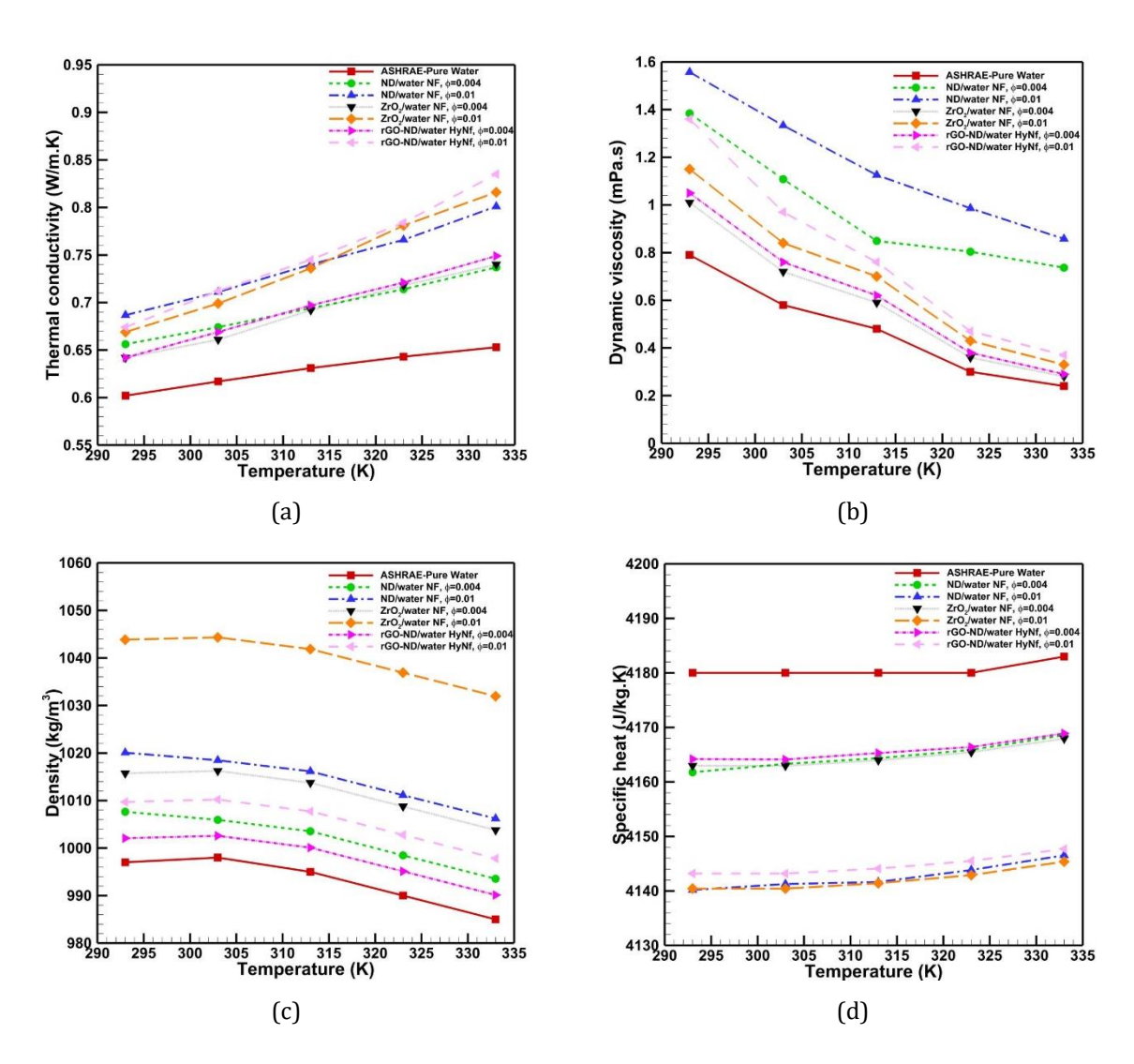


Fig. 2. Variations of the thermophysical properties of water-based NFs with the temperature

5. CFD Modeling

5.1. Pre-Processing

The turbulent kinetic energy and specific rate of dissipation at the walls are calculated by [44],

$$k = \frac{3}{2} (I |u_{ref}|)^2, \qquad \omega = \frac{k^{0.5}}{l \times C_{\mu}^{0.25}}$$
 (17)

Note that I represents the turbulence intensity, u_{ref} is reference velocity, which is the centerline velocity at the four nodes upstream of the first adiabatic step, C_{μ} is a constant (0.09), and l is the appropriate length scale. At the outlet, the pressure is uniform and fixed. The types of outflow velocity and temperature are inletOutlet and turbulence variables as zeroGradient.

5.2. Numerical Solver

OpenFOAM as an FVM-based open-source CFD software, is applied to solve the governing equations. With a completely open code and continuously improving algorithms, OpenFOAM is becoming a very prevalent and effective platform for CFD computations.

The pressure-velocity coupling problem is solved by using buoyantSimpleFoam in the object controlDict (for the steady-state fluid flow and heat transfer). In the object fvSchemes, the ddtSchemes, gradSchemes and divSchemes are set to Euler, Gauss linear and bounded Gauss upwind, respectively. In the object fvSolution, the residualControl and relaxationFactors are equal to 10^{-7} and 0.4, respectively. All simulations are accomplished using a Windows-based Desktop computer with a CPU Intel(R) Core i5, 2.9 GHz, and 8.00 GB RAM.

5.3. Post-Processing

The surface Nu number and average Nu number (Nuave) on the heated walls including the second step and two downstream walls are calculated as,

$$Nu(x) = \frac{hs}{k} = \frac{q \times s}{k \left(T_h - T_{ref}\right)}$$
 (18)

$$Nu_{ave} = \frac{\int_{L_1}^{L_2} Nu(x)dx}{L_2 - L_1} + \frac{\int_0^s Nu(y)dy}{s} + \frac{\int_{L_2}^L Nu(x)dx}{L - L_2}$$
(19)

The friction factor inside various DBFS channels with/without a baffle is estimated by,

$$f = \frac{2.0 \times \Delta P}{\rho_{nf} u_{ref}^2} \frac{s}{L} \tag{20}$$

For fully developed internal turbulent flow (electronic cooling), the value of FOM1 is determined as [51].

$$FOM1 = \frac{Mo_{nf}}{Mo_{bf}} = \frac{\rho_{nf}^{0.8} k_{nf}^{0.67} c_{p,nf}^{0.33}}{\mu_{nf}^{0.47}} \times \frac{\mu_{bf}^{0.47}}{\rho_{bf}^{0.8} k_{bf}^{0.67} c_{p,bf}^{0.33}}$$
(21)

Vajjha and Das [52] estimated the relative heat transfer rate (FOM2) versus temperature for different NFs and the base fluid as follows:

$$FOM2 = \frac{Mo_{nf}}{Mo_{bf}} \propto \frac{h_{nf}}{h_{bf}}$$

$$= \frac{\rho_{nf}^{0.8} k_{nf}^{0.5} c_{p,nf}^{0.5}}{\mu_{nf}^{0.3}} \times \frac{\mu_{bf}^{0.4}}{\rho_{bf}^{0.8} k_{bf}^{0.6} c_{p,bf}^{0.4}}$$
(22)

Yu et al. [53] defined the heat transfer enhancement criteria for NFs over their base fluids based on three distinct considerations: Re number, flow velocity, and pumping power. The constant Re number comparison is commonly used in the literature for the NF heat transfer enhancement and it implies the following flow velocity ratio,

$$\frac{U_{nf}}{U_{bf}} = \left(\frac{\rho_{bf}}{\rho_{nf}}\right) \times \left(\frac{\mu_{nf}}{\mu_{bf}}\right), \quad Re_{nf} \sim Re_{bf}$$
 (23)

This ratio for the constant Re number comparison is greater than unity, and it is a misleading characteristic in the heat transfer comparison. Yu et al. [53] claimed that it distorts the physical situation, and therefore, should not be used.

For the constant flow velocity comparison, FOM3 is defined as the Mo number ratio, and it is expressed as,

$$FOM3 = \frac{Mo_{nf}}{Mo_{bf}} = \frac{\rho_{nf}^{0.8} k_{nf}^{0.6} c_{p,nf}^{0.4}}{\mu_{nf}^{0.4}} \times \frac{\mu_{bf}^{0.4}}{\rho_{hf}^{0.8} k_{hf}^{0.6} c_{p,hf}^{0.4}}, \quad U_{nf} \sim U_{bf}$$
(24)

$$PEC_{baffle} = \frac{\frac{Nu_{DBFS1,2}}{Nu_{DBFS0}}\Big|_{\phi = const}}{\left[\frac{f_{DBFS1,2}}{f_{DBFS0}}\right]^{\frac{1}{3}}\Big|_{\phi = const}}$$
(25)

$$PEC_{nf} = \frac{\frac{Nu_{nf}}{Nu_{bf}}\Big|_{DBFS0,1,2}}{\left[\frac{f_{nf}}{f_{bf}}\right]^{\frac{1}{3}}}\Big|_{DBFS0,1,2}$$
(26)

$$PEC_{tot} = \frac{\frac{Nu_{nf,DBFS1,2}}{Nu_{bf,DBFS0}}}{\left[\frac{f_{nf,DBFS1,2}}{f_{bf,DBFS0}}\right]^{\frac{1}{3}}}$$
(27)

6. Results and Discussion

6.1. Validations and Mesh Independence Test

Rana et al. [54] numerically studied the effects of various water-based NFs on the laminar forced convection flow in a DBFS channel under fixed heat flux imposed at lower walls. In Figure 3, a comparative analysis of the influence of the volume fraction of ZnO nanoparticles on the surface Nu number is done at Re=225. The maximum discrepancy between the present study and Rana et al. [54] is less than 11.0%.

Applying a 3D particle-tracking velocimeter (PTV), Kasagi and Matsunaga [55] measured all three velocity components in turbulent separated and reattaching flow (isothermal) downstream of a BFS channel.

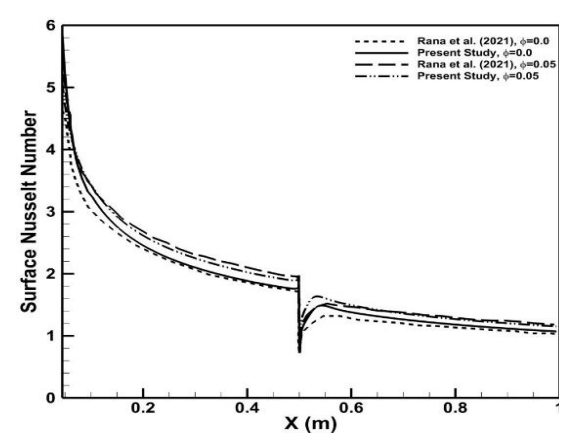


Fig. 3. Validation of the laminar forced convection flow in a DBFS channel without a baffle in terms of surface Nu number at Re=225

In Figure 4, we apply the LES in OpenFOAM to validate the vertical distribution of mean streamwise velocities at various horizontal stations.

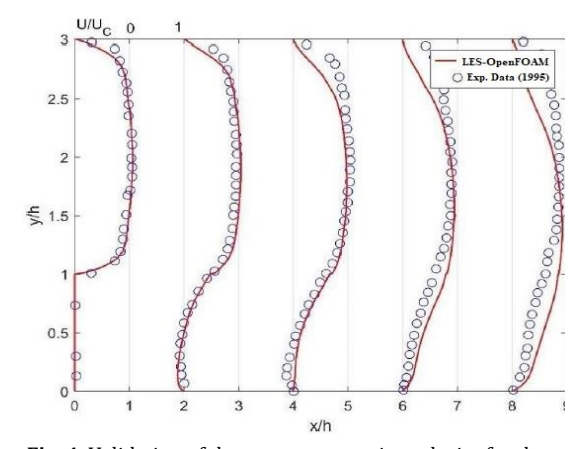


Fig. 4. Validation of the mean streamwise velocity for the turbulent isothermal flow of water over a BFS channel

Avancha and Pletcher [56] numerically examined the heat transfer and fluid mechanics of a turbulent separating and reattaching flow over a BFS. Near-wall region plots of spanwise and time-averaged temperature at various streamwise locations are validated in Figure 5 by applying the LES in OpenFOAM.

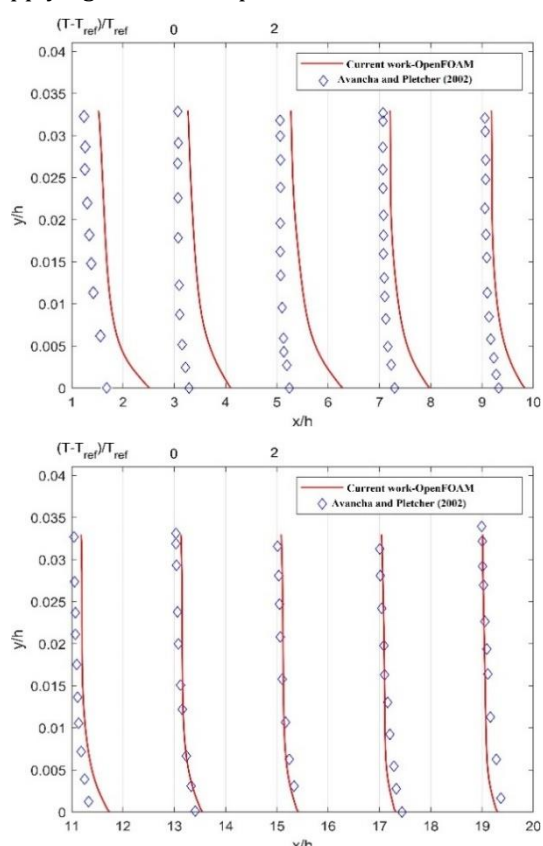


Fig. 5. Validation of the mean temperature in the nearwall region for turbulent forced convective heat transfer of air over a BFS channel

In Figure 6, the grid optimization tests for the turbulent forced convective heat transfer of the base fluid (pure water) over the DBFS0 configuration (with no baffle) are visualized in terms of the surface Nu number. It is seen that as the number of grids increases from 76846 (medium mesh) to 136044 (fine mesh), the Nu_{ave} is changed by less than 1.0%.

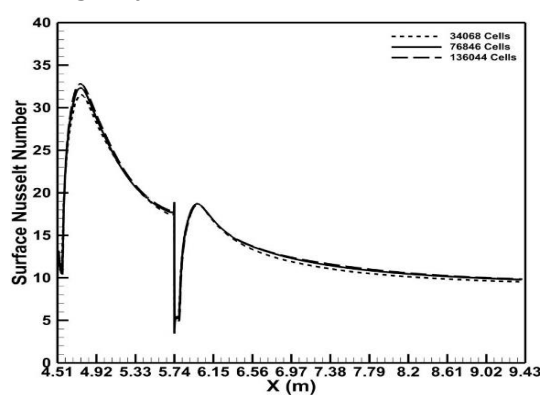


Fig. 6. Mesh independence tests for the pure water fluid flow in the DBFS0 channel

Accordingly, the medium mesh size is selected in current computations. The details of the mesh refinement are given in Figure 7.

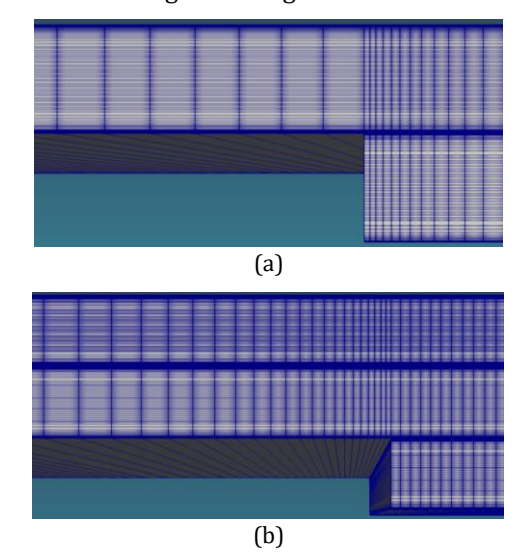


Fig. 7. Grid resolution in the streamwise (x) and wall normal (y) directions adjacent to the (a) first adiabatic step and (b) second hot step

6.2. FOM

In Figure 8, the temperature-dependent values of FOM1 for the water-based ND, ZrO₂, and rGO/ND single/hybrid NFs are obtained based on the correlation proposed by Sharma et al. [24] and experimental data.

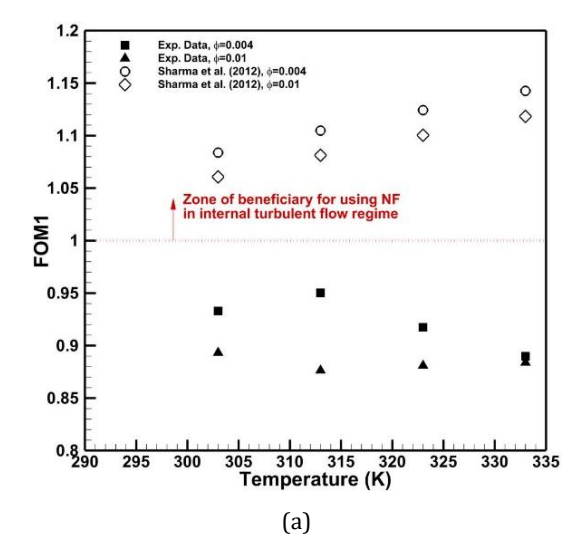
When the value of FOM1 is higher than 1.0, the zone of beneficiary for using NF in the single-phase turbulent forced convection flow is assured. As the NP loading increases from ϕ =0.004 to 0.01, the value of FOM1 diminishes.

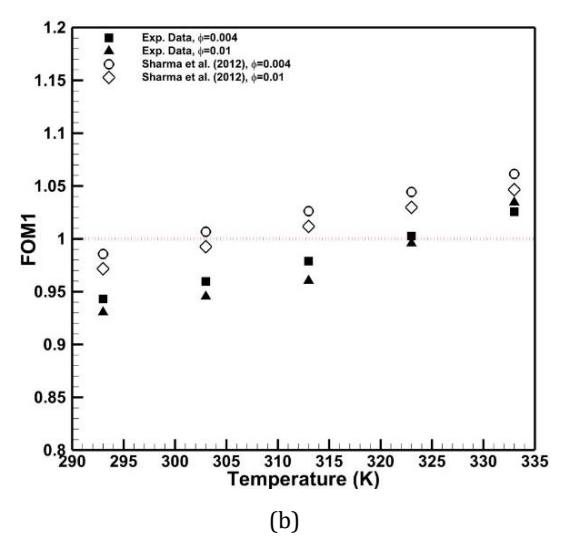
It indicates that the low-concentration NFs $(\phi=0.004)$ present superior heat transfer potential compared to their high-concentration counterparts $(\phi=0.01)$.

The relatively lesser dynamic viscosity and higher specific heat are obtained using the low-concentration NFs. It substantially enhances the value of FOM1. For the high-concentration NFs, however, the high thermal conductivity is balanced by a significant augmentation in the viscosity and density and a decline in the specific heat. Therefore, the value of FOM1 for the high-concentration NFs decreases compared to the low-concentration ones.

Additionally, using the ND/water NF, ZrO₂/water NF and water-based rGO/ND HyNf deteriorates the thermo-hydrodynamic performance (FOM1<1.0) compared to the pure water when the experimental data on the thermophysical properties are applied.

When the properties of water-based single/hybrid NFs are estimated by the regression (semi-empirical) correlations given by Sharma et al. [24], the value of FOM1 is overestimated.





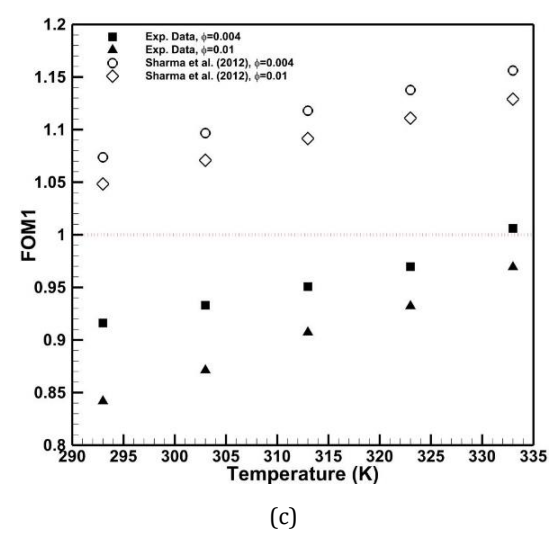


Fig. 8. Temperature-dependent variations of FOM1 for (a) ND/water NFs, (b) ZrO₂/water NF, and (c) water-based rGO/ND HyNf

The temperature-dependent variations of FOM2 and FOM3 for the above single/hybrid NFs are illustrated in Figure 9. Note that the thermophysical properties of NFs are obtained from the above experimental works.

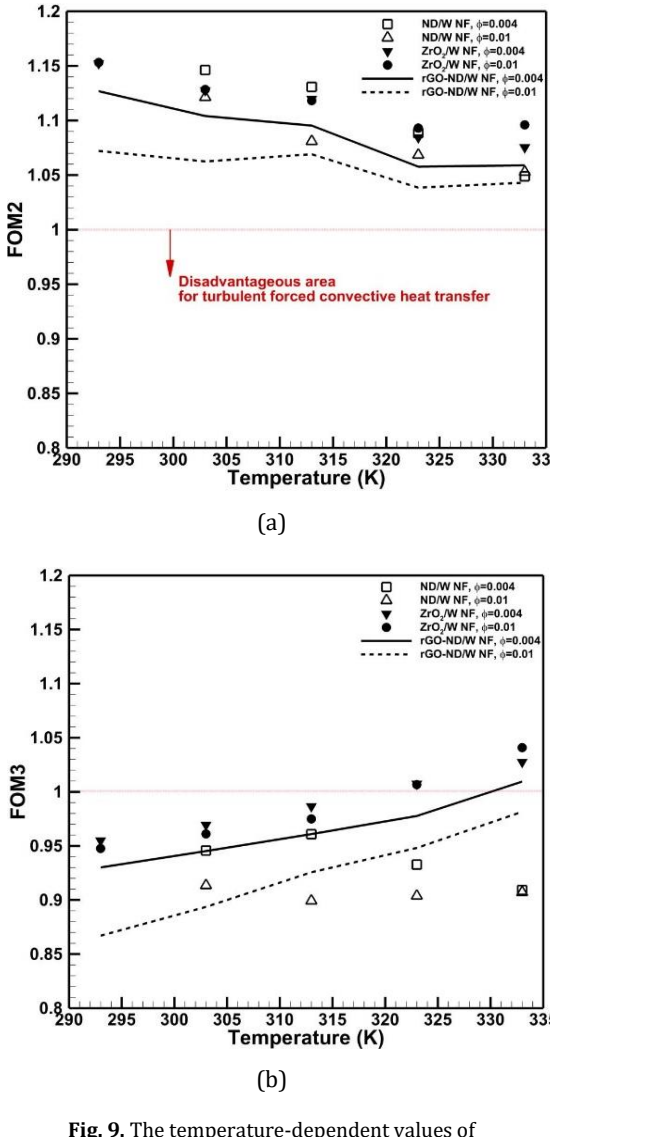


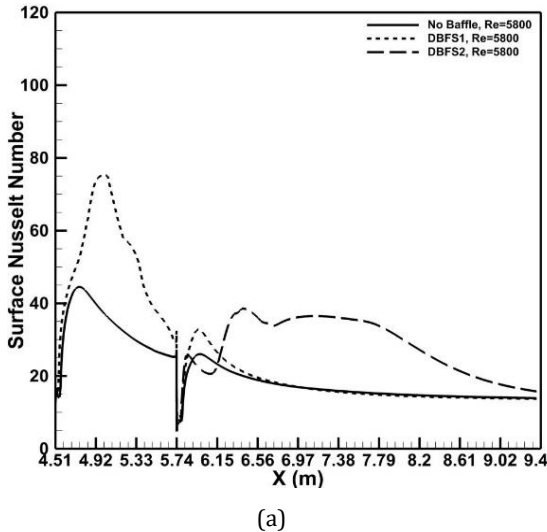
Fig. 9. The temperature-dependent values of (a) FOM2, and (b) FOM3.

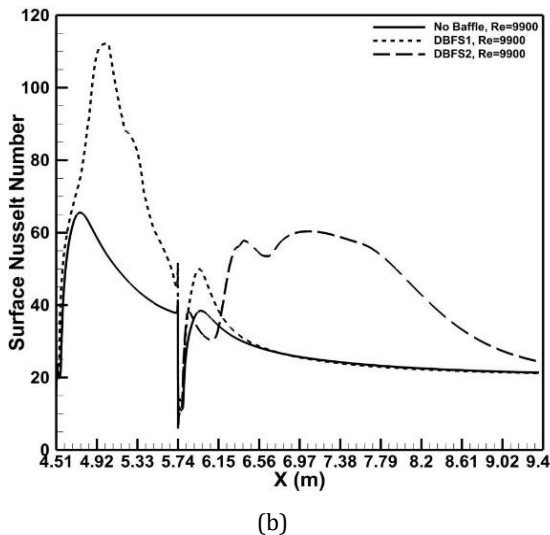
It is observed that the graphs of FOM2 proposed by Vajjha and Das [52] never cross the disadvantageous area for the single-phase turbulent forced convection heat transfer.

6.3. Pure Fluid

For the pure water, Figures 10a and 10b show the local variations of the Nu number along the heated surfaces due to the adiabatic baffle at Re=5800 and 9900, respectively. Close to the reattachment point, the flow collides with the bottom walls as a jet where isotherms compact. It results in the increased energy transfer.

In the downstream region from the reattachment point (on each hot wall), the heat transfer coefficient diminishes as the thickness of the TBL enlarges. The position of the impinging flow (jet-like) appears close to the streamwise position of Nu_{max} , as elucidated by Nie et al. [17].





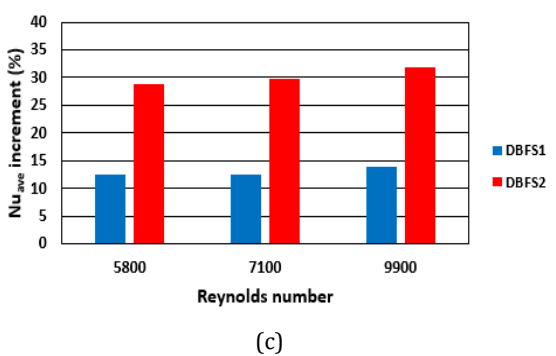


Fig. 10. Surface Nu number for the pure water flow over various DBFS channels at (a) Re=5800, (b) Re=9900 and (c) percentage of Nu_{ave} increment due to existence of baffle on the top adiabatic wall

In the present study, in the canonical case, the maximum Nu number develops close to the first adiabatic step. As the adiabatic baffle is installed over the first downstream wall (DBFS1) at Re=9900, the values of Nu_{max} over the first and second downstream walls enhance by 72% and 30%, respectively, compared to the BFS0 channel.

This is due to the phenomenon of the intensified vortex encapsulation generated by baffles in regions adjacent to steps (the first or second one). At Re=9900, the maximum Nu number over the first downstream wall moves downstream (along the streamwise direction from X=4.75m to X=5.0m) as the adiabatic baffle is added to the separated flow (DBFS1). In accordance with the result of Nie et al. [17], as the adiabatic baffle moves toward the first BFS, the magnitude of Nu_{max} enhances. Note that the presence of the adiabatic baffle over the second downstream wall does not increase the heat transfer capability (the heat exchange) of the forced convection flow over the first downstream wall. It is observed that by increasing the Re number, the local Nu number on the heated surfaces improves. As the Re number augments, the strength of the impinging jet on the bottom walls is intensified.

Considering the forced convection flow of the pure water in the DBFS1 channel, the increment of the Re number from 5800 to 9900 augments the value of Nu_{max} over the first downstream wall by 22%.

In Figure 10 c, the increment percentage of the average Nu number for the pure water due to the presence of an adiabatic baffle is determined. As can be observed, adding an adiabatic baffle enhances the heat transfer rate. Inserting an adiabatic baffle over the second heated downstream wall (the DBFS2 channel) significantly enhances the average Nu number (by 28-31%) in contrast to the canonical case. As discussed above, this improved heat transfer capability of the single-phase separated flow is only attributed to the intensified heat exchange over the second downstream wall.

As the baffle is positioned over the first downstream wall, the average Nu number improves by 12-14% compared to the DBFS0 channel.

Besides, the increment percentage of the average Nu number due to the adiabatic baffle is not sensitive to the range of the Re number investigated in this study.

6.4. Single/Hybrid NF

Figure 11 depicts the variations of the average Nu number for the single/hybrid NFs (ND, ZrO_2 , and rGO/ND) in various horizontal DBFS channels at various reference velocities (of the mainstream channel flow).

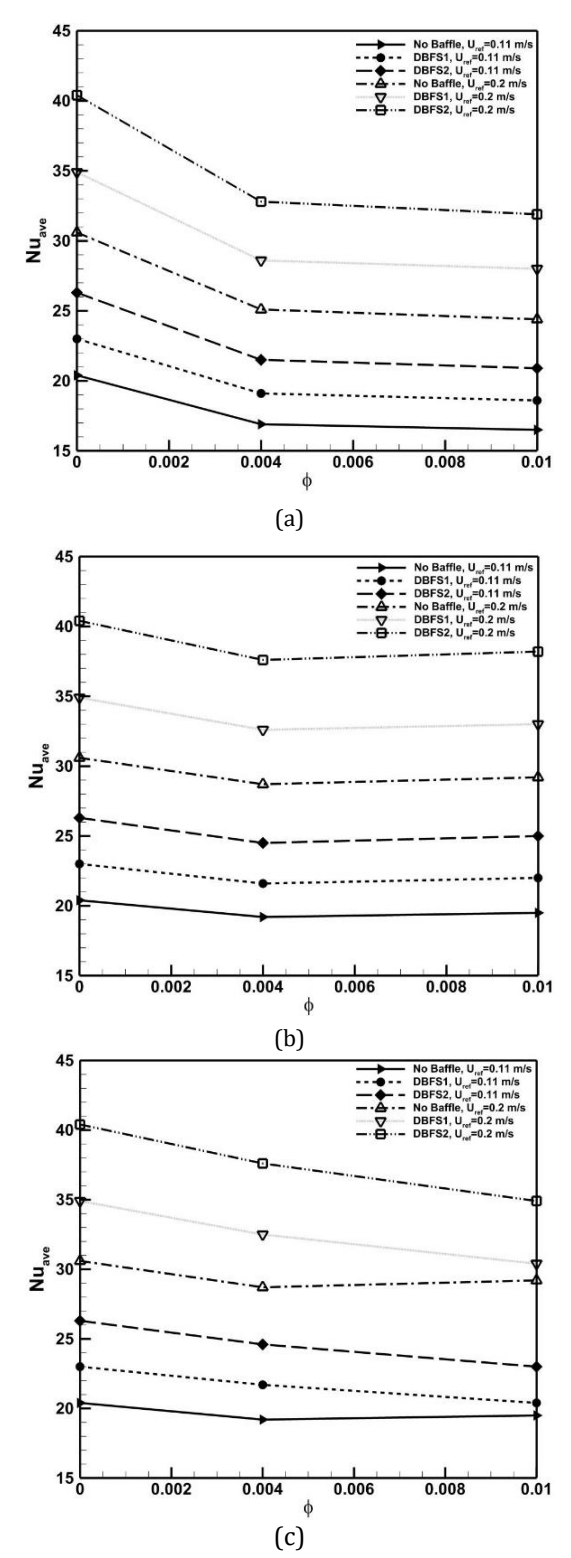


Fig. 11. Variations of the average Nu number for the (a) ND/water NF, (b) ZrO_2 /water NF, (c) water-based HyNf

As can be detected, the increment of the NP loading from ϕ =0.0 to 0.004 or 0.01 declines the heat transfer capability of the base fluid due to the negative effect induced by the increased viscosity on the forced convection performance. For example, in the canonical case (without a baffle), as the volume fraction of ND NPs in the base fluid increases from 0.0 to 0.004 and 0.01,

the average Nu number declines by 4.7% and 6.8%, respectively, at $U_{\rm ref}$ =0.11 m/s. Similarly, at $U_{\rm ref}$ =0.2 m/s, adding ND NPs reduces the average Nu number by 6.34% and 9%, respectively, in the DBFS0 channel.

It is realized that the average Nu number for the pure water or water-based single/hybrid NFs increases by increasing the velocity of the incoming flow in all DBFS channels.

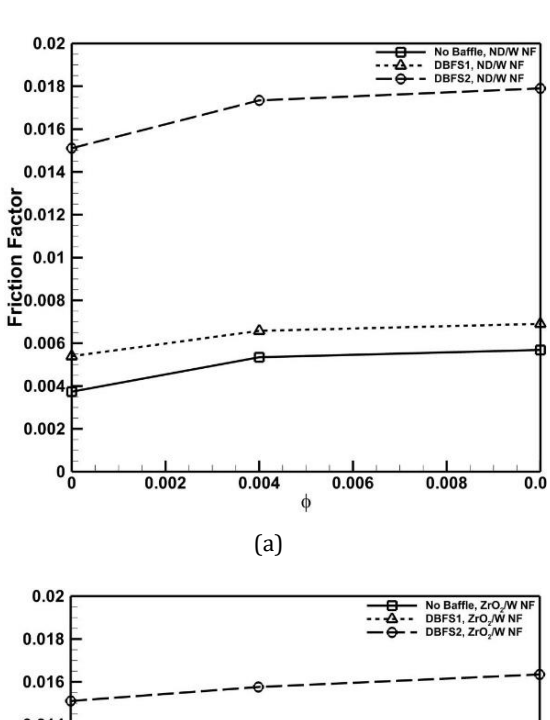
For example, for HyNf with ϕ =0.004 or 0.01, the average Nu number improves by 51-52% when the velocity of the incoming flow boosts by 70%. The flow interruption intensifies at higher velocities, and the swirling zone enlarges as well as the circulation region close to the baffle. The mixing of hot and cold fluids (the effectiveness of the heat dissipation) is intensified by increasing the velocity of the forced convection flow at the inlet.

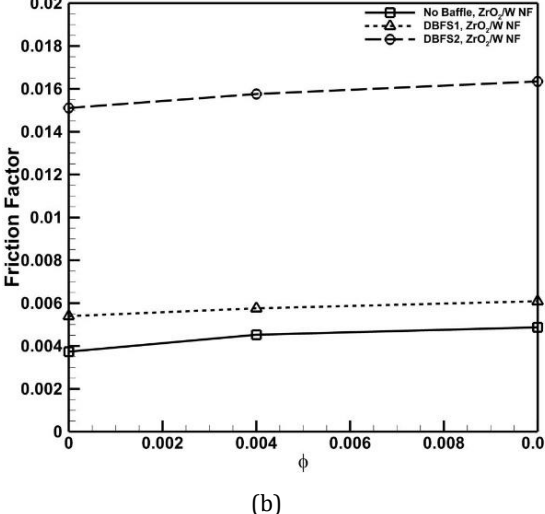
The effects of baffle position and volume fraction of single/hybrid NPs on the friction factor at U_{ref} =0.14 m/s are demonstrated in Figure 12. It is detected that the existence of an adiabatic baffle (positioned vertically downward from the top wall of the channel) noticeably augments the friction factor.

Considering the pure water flow, the application of an adiabatic baffle over the first (DBFS1) and second (DBFS2) downstream hot walls increases the friction factor by 43.24% and 304%, respectively, compared to the DBFS0 channel (without a baffle). It is due to the increment of the pressure drop imposed by the baffles. For the pure water flow in the DBFS0 channel, as the velocity of the incoming flow raises from 0.11 to 0.2, the friction factor abates by 20%. For the $ZrO_2/Water$ NF with φ =0.01 in the canonical channel, a 70% increment of the inlet velocity results in a 27% reduction in the friction factor.

Additionally, when the concentration of ND/water NF enhances from φ =0.0 to 0.004 and 0.01 in the DBFS2 channel, the friction factor increases by 14.56% and 17.88%, respectively. Since the penalty of increased pressure drop can lower the perks of using baffles and single/hybrid NFs in engineering and industrial systems, the value of PEC must be analyzed.

In Figure 13, the variations of PEC_{baffle} for the pure fluid and single/hybrid NFs at various reference velocities are illustrated. For the pure water or single/hybrid NF flows, substituting the DBFS0 configuration with the DBFS2 configuration is not advantageous $(0.7 < PEC_{baffle} < 0.9)$.





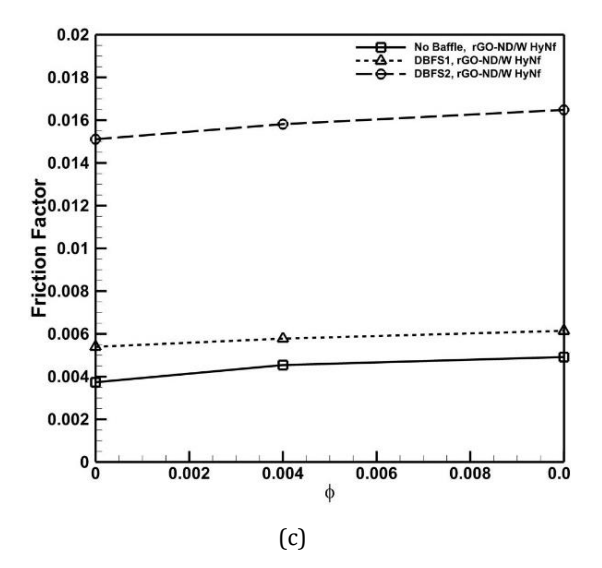


Fig. 12. Effects of baffle position on the friction factor for the pure water and single/hybrid NFs at $U_{\rm ref}$ =0.14 m/s

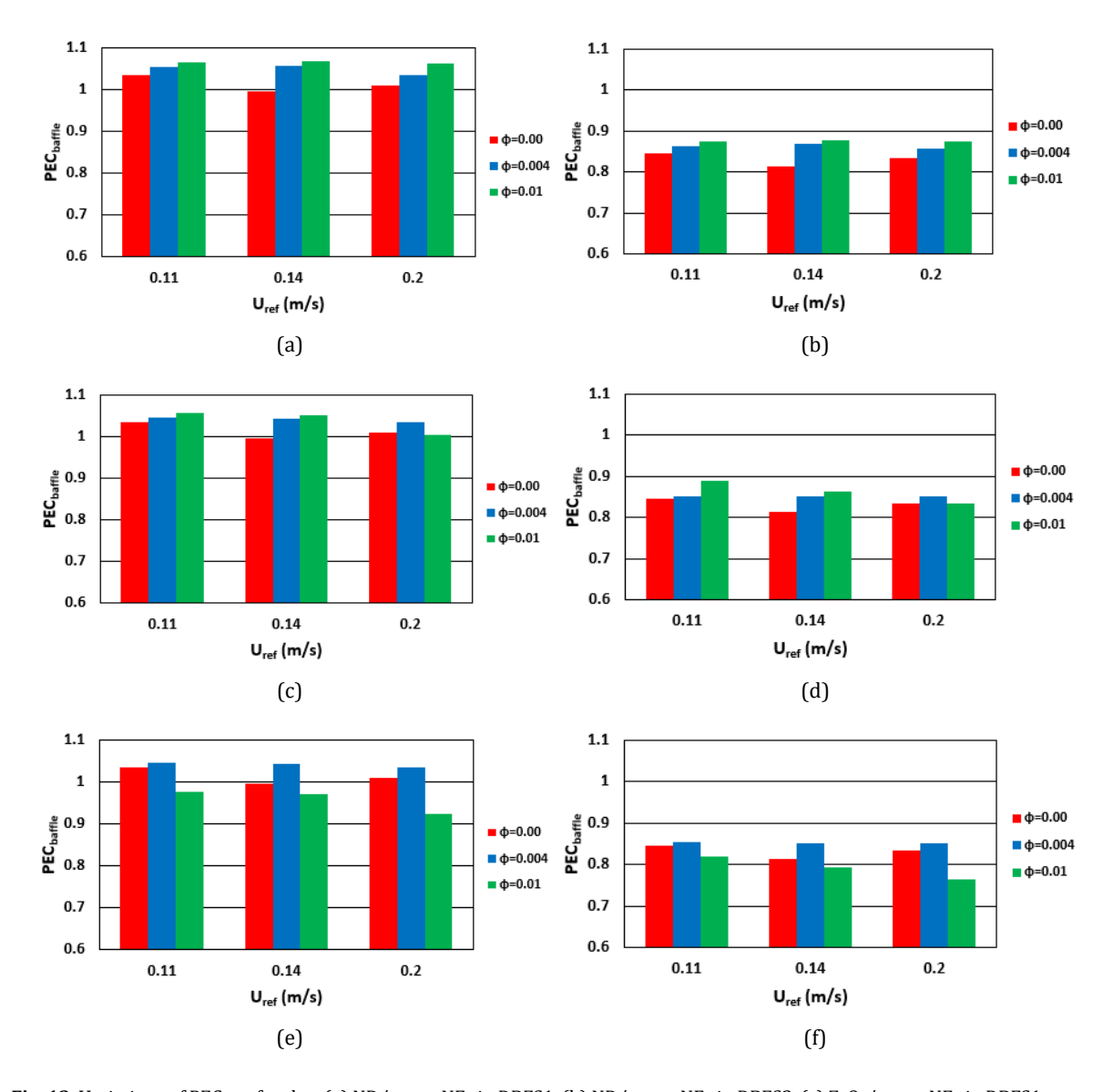


Fig. 13. Variations of PEC_{baffle} for the (a) ND/water NFs in DBFS1, (b) ND/water NFs in DBFS2, (c) ZrO₂/water NFs in DBFS1, (d) ZrO₂/water NFs in DBFS2, (e) HyNf in DBFS1, and (f) HyNf in DBFS2 at various velocities of the incoming flow

It indicates that the favorable effect (the intensified heat transfer) due to the addition of an adiabatic baffle over the second downstream wall cannot offset the negative effect (the rise in the pressure drop penalty).

For the ND/water and ZrO₂/water NFs, HyNf with φ=0.004 and the pure base fluid, when the DBFS0 configuration is replaced with the DBFS1 channel, favourable outcomes (PEC_{baffle}>1.0) are achieved.

• For the water-based rGO/ND HyNf with φ=0.01, even the DBFS1 channel cannot be prescribed because the viscosity of HyNf is the most dominating factor when the concentration slightly increases.

It is observed that the use of an adiabatic baffle in an effective position enhances the thermal efficacy of the separated forced convection flow where a disadvantageous heat transfer fluid (single/hybrid NF with a FOM1<1.0) is used.

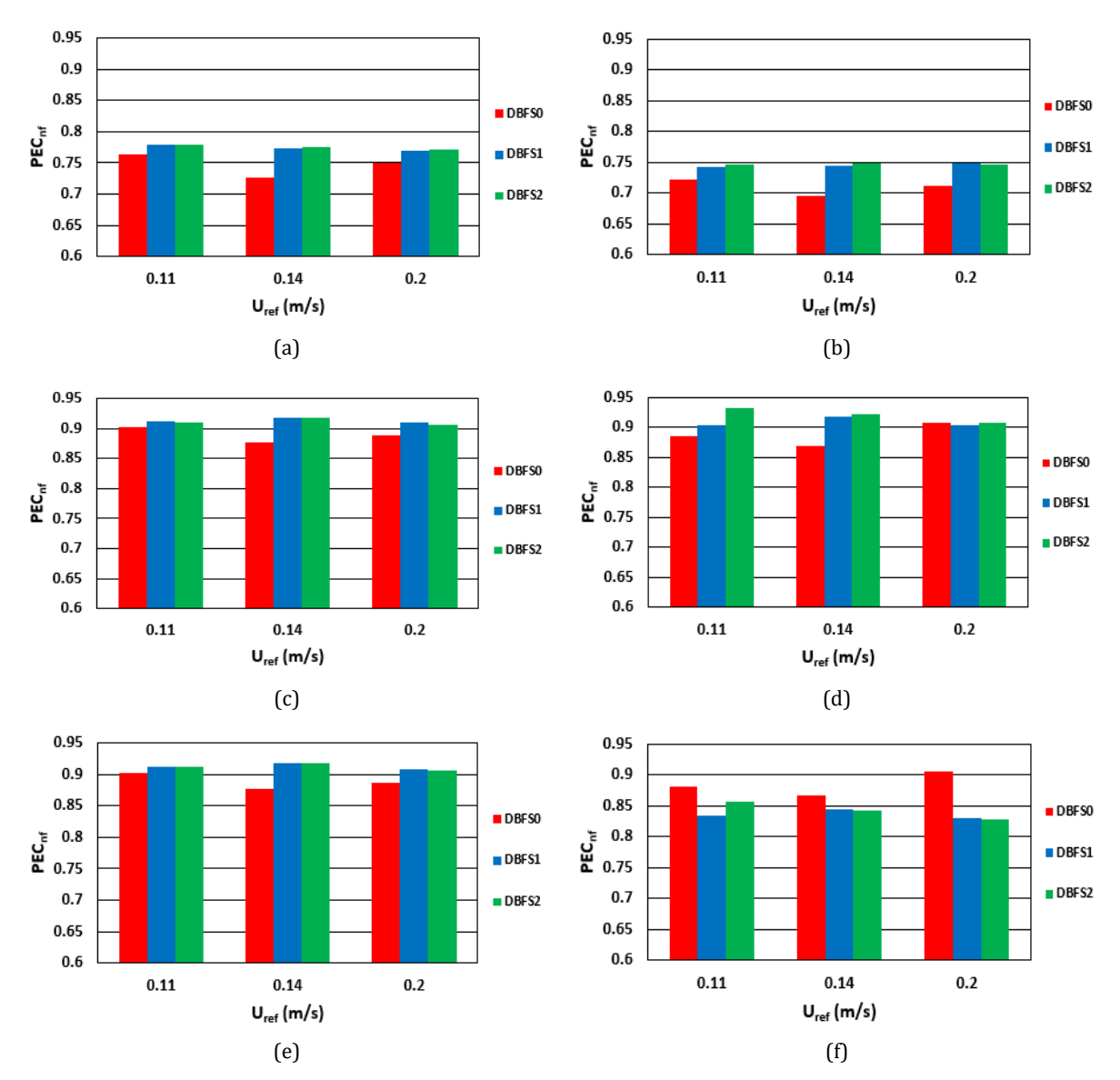


Fig. 14. Variations of PEC $_{\rm nf}$ for the (a) ND/water NFs with φ =0.004, (b) ND/water NFs with φ =0.01, (c) ZrO $_2$ /water NFs with φ =0.004, (d) ZrO $_2$ /water NFs with φ =0.01, (e) HyNf with φ =0.004, (f) HyNf with φ =0.01 at various velocities of the incoming flow

Moreover, for the ND/water NF with ϕ =0.004, 0.01, ZrO_2 /water NF with ϕ =0.004, 0.01, and water-based rGO/ND HyNf with ϕ =0.004, the application of a baffle over the first downstream hot wall is more beneficial (imposing a higher PEC_{baffle}) compared to the base fluid. So, adding an adiabatic baffle is more advantageous for less effective working fluids (with a FOM1<1.0).

The effects of adding single/hybrid NPs on the thermal performance of DBFS channels with/without a baffle are characterized by the PEC_{nf}, and they are visualized in Figure 14.

When the pure base fluid is substituted with the ND/water NF, $ZrO_2/water$ NF and water-based rGO/ND HyNf with φ =0.004 or 0.01 in the turbulent separated flow, the value of PEC_{nf} is lower than 1.0.

Besides, consistent with the results of FOM1, the thermal performance of ND/water NF is

significantly less than that of ZrO₂/water NF and water-based rGO/ND HyNf at all concentrations due to the higher viscosity of the ND/water NF.

The integrated effects of single/hybrid NPs and adiabatic baffles on the forced convection heat transfer in the DBFS channels are represented by PEC_{tot} , and they are given in Figure 15.

The simultaneous substitution of the base fluid in the DBFS0 configuration with the single/hybrid NF (with $\varphi{=}0.004$ or 0.01) in the DBFS1 or DFS2 channel is ineffective since the value of PECtot is lower than 1.0.

At the end, more numerical/experimental works must be performed to examine the convective heat transfer enhancement over complicated separated flows due to the introduction of appendages [57].

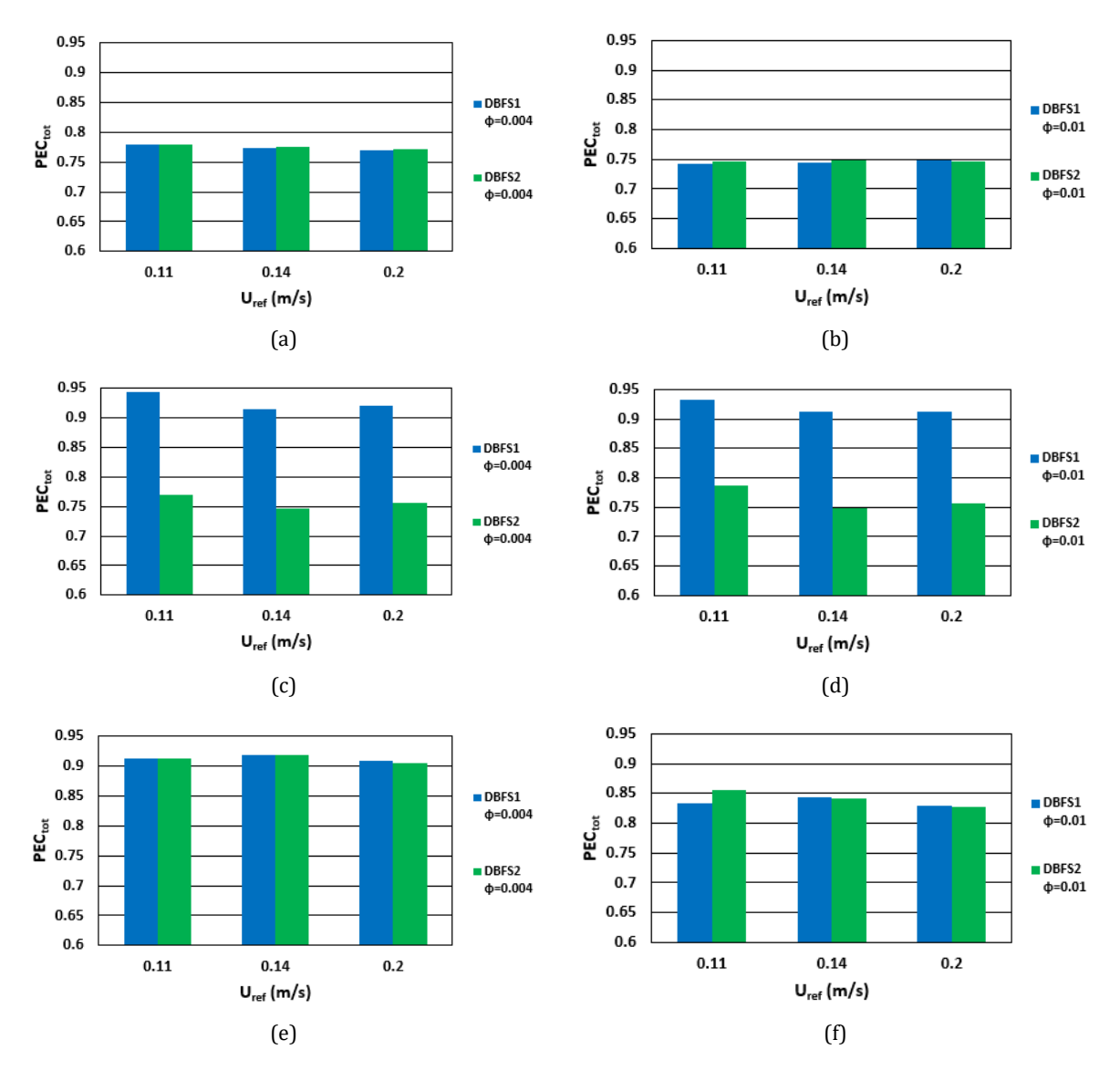


Fig. 15. Variations of PEC_{tot} for the (a-b) ND/water NFs, (c-d) ZrO₂/water NFs, and (e-f) HyNf at various velocities of the incoming flow

7. Conclusions

The outcomes of this research offered necessary insight into the sensitivity of a DBFS flow (with a fixed streamwise step separation) to adiabatic baffle and water-based single/hybrid NFs. The thermophysical properties of NFs were temperature-dependent, and they were acquired from the available lab-scale experiments in the literature. We showed the real possibility to enhance the heat transfer performance over this important configuration.

The key findings were established as follows:

(1) When the semi-empirical correlations were used for estimating the thermal conductivity and viscosity of single/hybrid NFs, the value of FOM1 became higher than 1.0. However, the NFs were not a good working fluid because the value of PEC_{nf} was lower than 1.0

- (2) The current study demonstrated how an irrelevant FOM (FOM2) confused us from the main message (disqualification of above single/hybrid NFs).
- (3) There was the phenomenon of the intensified vortex encapsulation generated by baffles in regions adjacent to steps (the first or second one). As the adiabatic baffle moved toward the first step, the magnitude of Nu_{max} was enhanced.
- (4) The mixing of hot and cold fluids (the effectiveness of the heat dissipation) was intensified by increasing the velocity of the forced convection flow. On the other hand, a 70% increment of the velocity of the incoming flow resulted in a 20-27% decrease in the friction factor.

- (5) At concentrations φ =0.004 or 0.01, the PEC_{nf} substantiated that the thermal performance of the ND/water NF was significantly lesser than that of other NFs. It was due to the higher viscosity of the ND/water NF.
- (6) The favorable effect (the intensified heat transfer performance) due to the addition of an adiabatic baffle over the second downstream wall did not offset the negative effect (the rise in the pressure drop penalty).
- (7) It was highly crucial to find the optimum position of the adiabatic baffle on the opposite wall even though the working fluids (NFs) with temperature-dependent properties were not a good coolant based on the value of the FOM1.

Future directions: We will explore the thermal efficacies of NFs in more complicated separated flows, such as shallow cavity flows with asymmetrical walls.

Nomenclature

c_p	Specific heat (J/kg·K)
d	Distance between step and baffle (m)
d_p	Nanoparticle diameter (m)
D	Normalized distance of baffle
F_1, F_2	Blending function
f	Friction factor
Н	Inlet height (m)
h_{baffle}	Baffle length (m)
h	Heat transfer rate (W/(m ² K))
I	Turbulence intensity
k	TKE $(m^2 \cdot s^{-2})$
k	Thermal Conductivity (Wm-1K-1)
l	Length scale of problem (m)
L	Total length (m)
L_1	Length of the inlet region (m)
L_2	Location of second step (m)
Мо	Mouromtseff number
Nu	Nusselt number
P	Pressure (N/m²)
Pr	Prandtl number
q	Heat flux (W/m²)
Re	Reynolds number
S	Step height (m)
S_{ij}	Strain rate tensor (1/s)
T	Temperature (K)
u	Velocity (m/s)
U_c	Upstream centerline velocity (m/s)
X	Distance in streamwise direction (m)
Subscripts	
•	•

Average

Maximum

ave

max

min	Minimum
bf	Base fluid
,	Daoc Hara
nf	Nanofluid
t	Turbulent
ref	Reference
tot	Total
Greek symbols	

α	Thermal diffusivity (m ² .s ⁻¹)
Γ_1 , Γ_2	Constants
δ_{ij}	Kronecker delta
ε	Turbulence dissipation (m ² /s ³)
μ	Dynamic viscosity (kg.m ⁻¹ .s ⁻¹)
ν	Kinematic viscosity (m ² /s)
ρ	Density (kg/m³)
τ	Turbulent shear stress (Kg/m.s²)
ϕ	Volume fraction of NP
ω	Specific dissipation rate (s-1)

Backward facing step

Computational fluid dynamics

Abbreviations

BFS

CFD

DBFS	Double backward facing step
ER	Expansion ratio
FEM	Finite element method
FOM	Figure of merit
FVM	Finite volume method
HyNf	Hybrid nanofluid
LES	Large eddy simulation
MTC	Maximum temperature constraint
MWCNT	Multi-walled carbon nanotubes
ND	Nanodiamond
NF	Nanofluid
NP	Nanoparticles
PEC	Performance evaluation criterion
PEP	Performance evaluation parameter
PIV	Particle image velocimetry
PTV	Particle-tracking velocimeter
RANS	Reynolds-Averaged Navier-Stokes
rGO	Reduced graphene oxide
SSA	Specific surface area
SST	Shear stress transport
TBL	Thermal boundary layer
TKE	Turbulent kinetic energy
UDD	Ultra-dispersed diamond
	ER FEM FOM FVM HyNf LES MTC MWCNT ND NF NP PEC PEP PIV PTV RANS rGO SSA SST TBL TKE

Funding Statement

This research did not receive any specific grant from funding agencies in the public, commercial, or not-for-profit sectors.

Conflicts of Interest

The authors declare that there is no conflict of interest regarding the publication of this article.

Authors Contribution Statement

Mahmoud Jourabian: Conceptualization; Data Curation; Formal Analysis; Investigation; Visualization; Roles/Writing – Original Draft; Writing; Review; Editing.

Mehrdad Raeesi: Software; Validation.

References

- [1] Tinney, C.E., Ukeiley, L.S., 2009. A study of a 3-D double backward-facing step. *Experiments in Fluids, 47*, pp. 427-438.
- [2] Rao, A.N., Zhang, J., Minelli, G., Basara, B., Krajnovic, S., 2019. Qualitative assessment of the bi-stable states in the wake of a finite-width double backward facing step. *Journal of Wind Engineering & Industrial Aerodynamics*, 186, pp. 241-249.
- [3] Abdulrazzaq, T., Togun, H., Alsulami, H., Goodarzi, M., Safaei, M.R., 2020. Heat transfer improvement in a double backward-facing expanding channel using different working fluids. *Symmetry*, *12*, p. 1088.
- [4] McQueen T., Burton D., Sheridan J., Thompson M.C., 2022. The double backward-facing step: interaction of multiple separated flow regions. *Journal of Fluid Mechanics*, 936, p. A29.
- [5] Mohankumar, V., Prakash, K.A., 2024. Numerical investigation of fluid flow and heat transfer characteristics over double backward-facing step with obstacles. *Heat Transfer Engineering*, 45, pp. 779-799.
- [6] Bahrami, H.R., Ghaedi, M., 2024. Enhancement of thermal energy transfer behind a double consecutive expansion utilizing a variable magnetic field. *Scientific Reports*, 14, 10236.
- [7] Rashid, F.L., Eleiwi, M.A., Tahseen, T.A., Mohammed, H.I., Tuama, S.A., Ameen, A., Agyekum, E.B., 2025. Influence of adiabatic semi-circular grooved in backward-facing step on thermal-hydraulic characteristics of nanofluid. *International Journal of Thermofluids*, 26, pp. 101052.
- [8] Akhter, R., Ali, M.M., Billah, Md.M., Uddin, Md.N., 2023. Hybrid-nanofluid mixed convection in square cavity subjected to oriented magnetic field and multiple rotating rough cylinders. *Results in Engineering*, 18, p. 101100.
- [9] Dehghan, P., Keramat, F., Mofarahi, M., Lee, C.H., 2023. Computational fluid dynamic analysis of graphene oxide/water nanofluid heat transfer over a double backward-facing

- microchannel. *Journal of the Taiwan Institute* of Chemical Engineers, 145, p. 104821.
- [10] Miri, R., Mliki, B., Ayed, L., AmmarAbbassi, M. Djebali, R., Hidouri, A., 2024. Numerical study of magnetohydrodynamic forced convective nanoliquid flow through a channel with backward facing step and three hot cylinder blocks. *Journal of Nanofluids*, 13, pp. 889-906.
- [11] Bahrami, H.R., 2021. Numerical investigation of flow and heat transfer behind a two-dimensional backward-facing step equipped with a semi-porous baffle. *Journal of Central South University*, 28, pp. 3354-3367.
- [12] Talaei, H., Bahrami, H.R., 2023. Backward-facing step heat transfer enhancement: a systematic study using porous baffles with different shapes and locations and corrugating after step wall. *Heat Mass Transfer*, 59, pp. 2213-2230.
- [13] Ma, Y., Ren, F., Tang, H., Wang, C., 2024. Vortex synchronization-enabled heat-transfer enhancement in a channel with backward- and forward-facing steps. *Physics of Fluids*, *36*, p. 033616.
- [14] Akhter, R., Ali, M.M., Alim, M.A., 2024. Data analysis of thermal performance and irreversibility of convective flow in porouswavy channel having triangular obstacle under magnetic field effect. *Heliyon, 10*, e34580.
- [15] Jahin, A.S. Samin, J.H., Chhoa, M.F., Faisal, F., Nokib, M.H.I., Rabby, M.I.I., 2025. Computational study of thermofluidic characteristics of Al2O3-Cu hybrid nanofluids in backward facing step channel with varying step angles. *Heliyon*, 11(4), e42638.
- [16] Hameed, S., Saha, S., 2024. Thermo-entropy analysis of water- FMWCNT nano-fluid flow in a backward-facing channel with obstacle. *Journal of Taibah University for Science, 18*, p.2314801.
- [17] Nie, J.H., Chen, Y.T., Hsieh, H.T., 2009. Effects of a baffle on separated convection flow adjacent to backward-facing step. *International Journal of Thermal Sciences, 48*, pp. 618-625.
- [18] Heshmati, A., Mohammed, H.A., Darus, A.N., 2014. Mixed convection heat transfer of nanofluids over backward facing step having a slotted baffle. *Applied Mathematics and Computation*, 240, pp. 368-386.
- [19] Alkumait, A.A.R., Zaidan, M.H., Ibrahim, T.K., 2018. Numerical investigation of forced convection flow over backward facing step

- affected by a baffle position. *Journal of Advanced Research in Fluid Mechanics and Thermal Sciences*, *52*, pp. 33-45.
- [20] Li, C., Cui, G., Zhai, J., Chen, S., Hu, Z., 2020. Enhanced heat transfer and flow analysis in a backward-facing step using a porous baffle. *Journal of Thermal Analysis and Calorimetry*, *141*, pp. 1919-1932.
- [21] Eslami, G., Karbalaei, A., 2021. On the optimum conditions for baffle installation in the backward facing step flow for maximization of the baffle performance. *Thermophysics and Aeromechanics, 28*, pp. 771-790.
- [22] Moayedi, H., 2021. Numerical analysis of the effect of baffle on heat transfer enhancement nanofluid flow over a backward facing step: A correlation for the average Nusselt number. *Amirkabir Journal of Mechanical Engineering*, 53, pp. 1021-1024.
- [23] Rana, S., Dura, H.B, Bhattrai, S. Shrestha, R., 2022. Impact of baffle on forced convection heat transfer of CuO/water nanofluid in a micro-scale backward facing step channel. *Journal of Thermal Engineering, 8*, pp. 310-322.
- [24] Sharma, K.V. Sarma, P.K., Azmi, W.H., Mamat, R., Kadirgama, K., 2012. Correlations to predict friction and forced convection heat transfer coefficients of water based nanofluids for turbulent flow in a tube. International Journal of Microscale and Nanoscale Thermal and Fluid Transport Phenomena, 3, pp. 1-25.
- [25] Palm, S.J., Roy, Nguyen, G.C.T., 2006. Heat transfer enhancement with the use of nanofluids in radial flow cooling systems considering temperature-dependent properties. *Applied Thermal Engineering*, 26, pp. 2209-2218.
- [26] Sundar, L.S., Shaik, F., Ahmed, M.J.B., 2023. Figures-of-merit analysis using the thermophysical properties of water and ethylene glycol based reduced graphene oxide/nanodiamond hybrid nanofluids. *Journal of Nanofluids*, 12, pp. 853-866.
- [27] Prabakar, K.S., Nagarajan, P.K., Venkatesan, J., Suseel Jai Krishnan, S., Sharifpur, M., 2023. Thermo-convective behavior and entropy generation studies on Alumina and Titania nanofluids flowing through polygonal ducts. *International Journal of Thermal Sciences*, 186, p. 108123.
- [28] Leena, M. Srinivasan, S., 2018. Experimental investigation of the thermophysical properties of TiO₂/propylene glycol-water

- nanofluids for heat transfer application. *Journal of Engineering Physics and Thermophysics*, 91, pp. 498-506.
- [29] Bianco, V., Manca, O., Nardini, S., 2014. Performance analysis of turbulent convection heat transfer of Al₂O₃ waternanofluid in circular tubes at constant wall temperature. *Energy*, *77*, pp. 403-413.
- [30] Xuan, Z., Wang, S., Zhai, Y., Wang, H., 2023. Thermodynamic performance of Al₂O₃-Cu-CuO/water (W) ternary nanofluids in the full-flow regime of convective heat transfer. *Experimental Thermal and Fluid Science*, 147, p.110959.
- [31] Rejvani, M., Alipour, A., Vahedi, S.M., Chamkha, A.J., Wongwises, S., 2019. Optimal characteristics and heat transfer efficiency of SiO2/water nanofluid for application of energy devices: A comprehensive study. *International Journal of Energy Research*, 43, pp. 8548-8571.
- [32] Ahmad, F., Mahmud, S., Ehsan, M.M., Salehin, M., 2023. Numerical assessment of nanofluids in corrugated minichannels: flow phenomenon and advanced thermohydrodynamic analysis. International *Journal of Thermofluids*, 20, p.100449.
- [33] Colla, L., Fedele, L., Scattolini, M., Bobbo, S., 2012. Water-based Fe₂O₃ nanofluid characterization: thermal conductivity and viscosity measurements and correlation. *Advances in Mechanical Engineering, 4*, p.674947.
- [34] Ho, C.J., Chang, C.Y., Cheng, C.Y., Cheng, S.J., Guo, Y.W., Hsu, S.T., Yan, W.M. 2016. Laminar forced convection effectiveness of Al₂O₃-water nanofluid flow in a circular tube at various operation temperatures: Effects of temperature-dependent properties. *International Journal of Heat and Mass Transfer*, *100*, pp. 464-481.
- [35] Kumar, V., Pare, A., Tiwari, A.K. Ghosh, S.K. 2021. Efficacy evaluation of oxide-MWCNT water hybrid nanofluids: an experimental and artificial neural network approach. *Colloids and Surfaces A: Physicochemical and Engineering Aspects, 620*, p. 126562.
- [36] Jasak, H., 2009. OpenFOAM: open source CFD in research and industry. International *Journal of Naval Architecture and Ocean Engineering*, 1, pp. 89–94.
- [37] OpenFOAM. OpenFOAM v6. https://openfoam.org/release/6/.
- [38] Jourabian, M., Raeesi, M., 2023. Turbulent forced convection flow of water-based

- nanofluids with temperature-dependent properties over backward-facing step channel with upwardly deflected downstream wall. *Numerical Heat Transfer, Part A: Applications, 86(1),* pp. 1-30.
- [39] Moradi, F. Pournaderi, P., Omidvar, P., 2024. Magnetohydrodynamic flow of nanofluid through backward-facing step micro- and minichannels: A comparative analysis of single-phase and two-phase approaches. *Numerical Heat Transfer, Part A: Applications*, pp. 1-22.
- [40] Sekrani, G., Poncet, S., Proulx, P., 2018. Modeling of convective turbulent heat transfer of water-based Al₂O₃ nanofluids in an uniformly heated pipe. *Chemical Engineering Science*, 176, pp. 205-219.
- [41] Togun, H., Safaei, M.R., Sadri, R., Kazi, S.N., Badarudin, A., Hooman, K., Sadeghinezhad, E., 2014. Numerical simulation of laminar to turbulent nanofluid flow and heat transfer over a backward-facing step. *Applied Mathematics and Computation, 239*, pp. 153–170.
- [42] Loksupapaiboon, K., Suvanjumrat, C., 2023. Forced convective heat transfer and fluid flow past a rotating hand-shaped former for improving rubber glove curing. *Case Studies in Thermal Engineering*, 47, p. 103050.
- [43] Menter, F.R., 1994. Two-equation eddyviscosity turbulence models for engineering applications. *American Institute Aeronatics* and *Austronatics Journal*, *32*, pp. 1598-1605.
- [44] Menter, F.R., Kuntz, M., Langtry, R., 2003. Ten years of industrial experience with the SST turbulence model. *Turbulence, heat and mass transfer*, 4(1), *Begell House Inc*, pp. 625-632.
- [45] Asnaghi, A., Svennberg, U., Bensow, R.E., 2019. Evaluation of curvature correction methods for tip vortex prediction in SST k- ω turbulence model framework. *International Journal of Heat and Fluid Flow, 75*, pp. 135-152.
- [46] You, Y., Seibold, F., Wang, S., Weigand, B., Gross, U., 2020. URANS of turbulent flow and heat transfer in divergent swirl tubes using the k- ω SST turbulence model with curvature correction. *International Journal of Heat and Mass Transfer*, 159, p. 120088.
- [47] Shuvo, M.S., Ruvo, T.H., Saha, S., 2023. Characteristics of turbulent forced convective nanofluid flow and heat transfer in a 2D axisymmetric corrugated pipe. *Thermal Science and Engineering Progress*, 41, p. 101838.

- [48] Alklaibi, A.M., Sundar, L.S. Sousa, A.C.M., 2021. Experimental analysis of exergy efficiency and entropy generation of diamond/water nanofluids flow in a thermosyphon flat plate solar collector. *International Communications in Heat and Mass Transfer*, 120, pp. 105057.
- [49] Sundar, L.S., Sambasivam, S., Mewada, H.K., 2022. ANFIS modelling with fuzzy C-mean clustering of experimentally evaluated thermophysical properties of zirconia-water nanofluids. *Journal of Molecular Liquids*, *364*, p. 119987.
- [50] ASHRAE, Handbook, 1985. Fundamentals, American Society of Heating, Refrigerating and Air-Conditioning Engineers Inc., Atlanta.
- [51] Simons, R.E., 2006. Comparing heat transfer rates of liquid coolants using the Mouromtseff number. *Electronics Cooling*, 12, pp.35-39.
- [52] Vajjha, R.S., Das, D.K., 2012. A review and analysis on influence of temperature and concentration of nanofluids on thermophysical properties, heat transfer and pumping power. *International Journal of Heat and Mass Transfer*, 55, pp. 4063-4078.
- [53] Yu, W., France, D.M., Timofeeva, E.V. Singh, D., Routbort, J.L., 2010. Thermophysical property-related comparison criteria for nanofluid heat transfer enhancement in turbulent flow. *Applied Physics Letters*, 96, p. 213109.
- [54] Rana, S., Dura, H.B., Bhattrai, S., Shrestha, R., 2021. Comparative study of thermal performance of different nanofluids in a double backward-facing step channel: a numerical approach, Hindawi International *Journal of Chemical Engineering*, 2021(1) p. 626343.
- [55] Kasagi, N., Matsunaga, A., 1995. Three-dimensional particle-tracking velocimetry measurement of turbulence statistics and energy budget in a backward-facing step flow. *International Journal of Heat and Fluid Flow*, 16, pp. 477-485.
- [56] Avancha, R.V.R., Pletcher, R.H., 2002. Large eddy simulation of the turbulent flow past a backward-facing step with heat transfer and property variations. *International Journal of Heat and Fluid Flow, 23*, pp. 601-614.
- [57] Nagarajan, P., Sundaram, S.S., 2024. The effect of appendages at step on heat transfer in a backward-facing step. *International Communications in Heat and Mass Transfer*, 155, p. 107589.